Published in final edited form as:
Nat Struct Mol Biol. 2015 October ; 22(10): 788–794. doi:10.1038/nsmb.3096.

Structure-based energetics of protein interfaces guide Foot-and-Mouth Disease virus vaccine design

Abhay Kotecha[#1], **Julian Seago**[#2], **Katherine Scott**[3], **Alison Burman**[2], **Silvia Loureiro**[5], **Jingshan Ren**[1], **Claudine Porta**[1,2], **Helen M. Ginn**[1], **Terry Jackson**[2], **Eva Perez-Martin**[2], **C. Alistair Siebert**[1], **Guntram Paul**[4], **Juha T. Huiskonen**[1], **Ian M. Jones**[5], **Robert M. Esnouf**[1], **Elizabeth E. Fry**[1], **Francois F. Maree**[3,6,†], **Bryan Charleston**[2,†], and **David I. Stuart**[1,7,†]

[1]Division of Structural Biology, University of Oxford, Oxford, UK

[2]The Pirbright Institute, Pirbright, UK

[3]Transboundary Animal Disease Programme, Agricultural Research Council-Onderstepoort Veterinary Institute, Onderstepoort, South Africa

[4]Merck Sharp & Dohme Animal Health, Cologne, Germany

[5]Animal and Microbial Sciences, University of Reading, Reading, UK

[6]Department of Microbiology and Plant Pathology, University of Pretoria, Pretoria, South Africa

[7]Life Science Division, Diamond Light Source, Didcot, UK

[#] These authors contributed equally to this work.

Summary

Virus capsids are primed for disassembly yet capsid integrity is key to generating a protective immune response. Here we devise a computational method to assess relative stability of protein-protein interfaces and use it to design improved candidate vaccines for two of the least stable, but globally important, serotypes of Foot-and-Mouth Disease virus (FMDV), O and SAT2. FMDV capsids comprise identical pentameric protein subunits held together by tenuous non-covalent

[†]Correspondence and requests for materials should be addressed to D.I.S. (dave@strubi.ox.ac.uk), F.F.M. (MareeF@arc.agric.za) or B.C. (bryan.charleston@pirbright.ac.uk).

Accession Codes
The coordinates and X-ray structure factors for the inactivated O1M and A22 mutant particles have been deposited with the RCSB Protein Data Bank under accession codes 5ddj, 5d8a, respectively and the EM structures for O1M and SAT2 mutant particles are deposited with Protein Data Bank accession codes 5ac9 and 5aca and in the EM Data bank under accession codes 3129 and 3130, respectively.

Author Contributions A.K., E.E.F., R.M.E., and D.I.S. developed MD simulation protocols, A.K., J.S., K.S., A.B., S.L. and C.P. prepared samples, J.R., H.M.G., J.T.H., E.P-M., G.P., C.A.S., F.F.M. and E.E.F. assisted in research. A.K., J.S., F.F.M., E.E.F. T.J., I.M.J, R.M.E., D.I.S. and B.C. designed the study, all authors analysed data and A.K., J.S., E.E.F., B.C. and D.I.S. wrote the manuscript.

Author Information
Readers are welcome to comment on the online version of the paper.

Competing Financial Interest
A number of the stabilising mutations are patented (patent number WO 2014154655 A1, patent holders: R.M.E., E.E.F., A.K. and D.I.S.) and work on a VLP based stabilised vaccine antigen is ongoing at Intervet (MSD Animal Health), in collaboration with the authors (except that F.F.M. and K.S. are not part of this ongoing work). This work was not funded by MSD Animal Health but by a Wellcome Trust Translation Award.

Europe PMC Funders Author Manuscripts

interactions, and are often unstable. Chemically inactivated or recombinant empty capsids, which could form the basis of future vaccines, are even less stable than live virus. We use a novel restrained molecular dynamics strategy, to rank mutations predicted to strengthen the pentamer interfaces to produce stabilized capsids. Structural analyses and stability assays confirmed the predictions, and vaccinated animals generated improved neutralising antibody responses to stabilised particles over parental viruses and wild-type capsids.

Foot-and-mouth disease virus (FMDV) is a small RNA virus, whose icosahedral capsid contains 60 copies each of proteins VP1–VP4. FMDV is responsible for a contagious, economically devastating livestock disease endemic in many developing regions of Asia, Africa and South America, with developed countries at risk of sporadic but serious outbreaks (e.g. UK 2001, Japan 2010 and Egypt 20121–3). Where endemic, disease control is predominantly by vaccination. There are seven serotypes of FMDV [A, O, C, Asia, and Southern African Territories (SAT) 1, 2, and 3]4 and each contains multiple and constantly evolving sub-serotype strains. A vaccine against one serotype does not protect against other serotypes or subtypes within a serotype, necessitating the continued development of new vaccine strains. The majority of vaccines produced worldwide are type O whereas SAT2 is the most prevalent serotype in sub-Saharan Africa5.

FMDV serotypes differ markedly in their capsid stability, A and Asia-1 being relatively stable, whereas O and SAT viruses are more sensitive to heat and pH6. Commercial vaccines are produced by chemical inactivation of virus particles, which renders them even less stable and above 30°C they rapidly convert into immunogenically incompetent pentameric subunits6, 7. Thus, vaccine integrity requires expensive, difficult-to-maintain cold chains and effective protection requires frequent immunisations5, 8. Recombinant empty capsids show promise as future vaccines as they overcome many of the disadvantages of preparing vaccines from live virus, however, they are even less stable than virus particles9.

Knowledge of the three-dimensional structure of viral capsids should allow rational engineering of their properties. Although four different serotypes of FMDV have been analysed in atomic detail10–14, few attempts have been made to engineer thermo-stable capsids15, 16. The pentameric sub-assemblies are highly stable, so stabilisation of the inter-pentamer interactions should be sufficient to enhance capsid stability, and the effectiveness of vaccine preparations. The introduction of a disulphide bond across the interface between adjacent pentamers enabled the production of thermo-stable FMDV empty-capsids for an A serotype (A22 Iraq)17. However, covalent stabilisation may not be compatible with virus viability or with the structure of all viruses16.

Here, we developed a molecular dynamics (MD) based strategy for the evaluation of mutations designed to increase capsid stability by increased non-covalent interactions, and applied it to the less stable serotypes O and SAT2, and the more stable A viruses. Structural analyses and stability assays confirmed that the method is predictive of increased stability. Furthermore, animals vaccinated with candidate mutant viruses generated improved neutralising antibody responses, demonstrating potential value for such stabilized vaccine antigens.

Europe PMC Funders Author Manuscripts

Results

FMDV capsids dissociate into pentameric sub-assemblies

Inactivated FMDV capsids dissociate into pentameric subunits at pH <7.0, temperatures >30°C1, 4, 6, 15, and on prolonged storage at 4°C (Figure 1a and 1b). We examined the interface between pentamers for opportunities to stabilise these inter-pentamer contacts by enhancing non-covalent interactions. From four different serotypes10, 11, 13, 14, 18 we identified 85 amino acids contributing to this interface: 57 from VP2 and 28 from VP3. VP2 shows ~80% sequence identity between different serotypes and we selected non-conserved, interface residues inaccessible to antibodies and thus unlikely to affect antigenicity (Supplementary Figure 1) for the introduction of potentially stabilising interactions (for each residue a range of mutants were possible). We focussed on the region close to the icosahedral 2-fold axis since enterovirus uncoating is known to initiate at this point and disorder of the N-terminus of VP2 adjacent to the 3-fold axis made this alternative region less reliable for modelling19–21. We chose O1/Manisa/Turkey/69 (O1M), a field strain widely used in current vaccines, and SAT2 ZIM/7/83 (SAT2) as our target antigens, and A22 Iraq 24/64 (A22) as a stable reference strain17. In the absence of high-resolution structures, O1BFS (PDB ID: 1BBT)22 was used as the model for O1M (98% sequence identity in capsid protein VP2) and SAT1 (PDB ID: 2WZR)14 as the model for SAT2 (78% identity in VP2). A panel of 12 potential stabilizing mutants within VP2 was proposed for O1M based on visual inspection of the structures, 4 of which were also chosen for SAT2 and the 2 most promising were chosen for A22 (Table 1) and these were modelled by *in silico* mutagenesis (program COOT23) and localised energy minimisation.

MD simulations and binding free-energy calculations

We devised a novel MD simulation protocol for the rapid evaluation of the relative stability potential of mutant viruses. Atomistic dynamics are usually applied to complete biological ensembles24, 25, however, in the context of small well-defined changes in a complex virus particle this approach has poor signal-to-noise ratio and is expensive computationally. We therefore reduced the complexity of the simulation, initially to two interfacial protomers (Figure 1c), which required a week of processing on 8 CPU cores (AMD Opteron 6174 at 2.2 GHz). Even so, artefacts made it difficult to detect small changes in the binding free-energy of the interface. Thus, a protocol was devised in which the model was further trimmed to atoms within 13 Å of the interface and positional restraints were applied which increased with distance from the interface. To enable this, non-physical “dummy” atoms were placed mid-way between pairs of interacting atoms along the contact interface centred on the icosahedral 2-fold axis of symmetry. During simulations restraints were defined such that atoms within 10 Å of any dummy atom were allowed to move freely whilst atoms more remote, and the dummy atoms themselves, were tightly restrained (Figure 1d). These restraints considerably simplified the simulation (~24h computation using the same AMD CPUs) and dramatically reduced the noise by ‘freezing’ unchanged parts of the structure, including the disconnected atoms at the periphery of the model. A set of negative controls was tested with the O1M model to validate the protocol whereby a salt-bridge or H-bond network was deliberately disrupted (Table 1); these mutations resulted in positive $\Delta\Delta G$

values. Note that such dynamics based methods cannot model additional covalent interactions, such as disulphide bonds.

Putative mutations that confer increased stability

The results of the free-energy calculations are shown in Table 1. Residue 93 of VP2 is part of an α-helix adjacent to the icosahedral 2-fold axis, and is largely conserved within but not between serotypes (Supplementary Figure 1 and Figure 1c, **right panel**). The relatively stable A serotype has a histidine at this position whose imidazole ring forms a hydrophobic stacking interaction with the corresponding symmetry-related moiety. Simulation results suggested that this virus could be further stabilised by mutation to tyrosine ($\Delta\Delta G$=-7.7 kcal/mol) or even better to phenylalanine ($\Delta\Delta G$=-10.3 kcal/mol). For O1M and SAT2, the simulations suggested that stability would be enhanced by mutation of the equivalent serine to histidine (S93H) ($\Delta\Delta G$=-7.7 and -5.3 kcal/mol, respectively) and further improved by mutation to tyrosine ($\Delta\Delta G$=-11.8 and -12.2 kcal/mol, respectively), whose side chain was suggested to hydrogen bond to the backbone of VP2 89. Nonetheless, a phenylalanine was predicted to confer even greater stability ($\Delta\Delta G$= -13.8 and -13.2 kcal/mol, respectively). Substitution with a bulky tryptophan was less effective ($\Delta\Delta G$= -9.5 kcal/mol for O1M), as were non-aromatic hydrophobic side chains (V, L, I and M) (Table 1). Some VP2 mutations away from the 2-fold axis produced stabilization (S97Q, S97I and to a lesser extent V90N), with Y98F predicted to be most effective ($\Delta\Delta G$= -10.3 and -5.6 kcal/mol for O1M and SAT2, respectively).

Mutant viruses are infectious and genetically stable

The effect of the amino-acid mutations was first tested in recombinant virus. Transcripts were electroporated or transfected into BHK-21 cells to generate infectious stocks. These stocks were then used to infect ZZ-R127 goat epithelium cells, which are highly susceptible to FMDV infection26. Subsequent passages in BHK-21 cells, commonly used in the production of FMD vaccines, were possible because the SAT2 virus was cell culture-adapted, whilst two VP3 mutations (H56R and D60G) were introduced in O1M, enabling cell entry via heparan sulphate27. These mutations, remote from the pentamer interface, did not affect the particle stability (Supplementary Figure 1) and are often present in vaccine strains. All recombinant viruses were sequenced after four passages, revealing no changes or obvious sub-populations. All produced clear, consistent, cytopathic effect (CPE), however differences were observed between viruses. The patterns of CPE and plaque sizes varied markedly and in general stabilised viruses gave substantially smaller plaques than the parental virus (Figure 2a). However, the yields of wild-type and mutant viruses were broadly similar (Supplementary Table 1). In addition to generating recombinant viruses, recombinant empty capsids containing the same amino acid substitutions were made using the mammalian and insect cell expression systems described previously17, 28.

Thermal and acid stability of engineered mutant viruses

Capsid stability was determined by fluorescent thermal stability assays29 at pH 7.5. For O1M, wild-type virus dissociated at 52.0°C, S93W was similar, whereas S93Y, S93F and Y98F dissociated at 53.5°C. Inactivated SAT2 followed this pattern: wild-type and S93W

capsids dissociating at similar temperature (47.0°C) whilst S93H and S93Y dissociated at higher temperatures, 51.0°C and 53.5°C, respectively (Figure 2b, Table S2). At lower pH (6.5), wild-type O1M capsids dissociated at 31.0°C whereas mutant capsids were more stable; S93W dissociated at 34.0°C, S98F and S97Q at 35.0°C, and S93Y and S93F at 38.0°C, (Supplementary Figure 1).

The stability of inactivated wild-type and S93Y O1M particles was assessed by negative-stain electron microscopy (EM). Immediately after purification ~90% of wild-type capsids were intact compared to almost 100% for S93Y (based on the mean particle count within five randomly selected areas of the grid). After 10 days storage at 4°C only ~20% of the wild-type capsids remained intact as compared to 90% for the mutant (Supplementary Figure 2). Finally, samples were incubated at 37°C for 5, 10 or 20 min and analysed by EM. Remarkably, only ~5% of the wild-type virions remained intact compared to ~60% for the mutant after 20 min incubation at 37°C (Supplementary Figure 2). An ELISA assay on infectious O1M virus, gave similar results. Wild-type or S93Y particles were incubated at 37°C for up to 72 h, and samples analysed using llama antibodies (VHH M170 recognising intact capsids and VHH M3 recognising pentamers)30. As expected, more than 50% of the S93Y capsids were intact after 72h versus only 15% of the wild-type (Supplementary Figure 2). In conclusion, the mutant viruses were consistently more stable at elevated temperatures and at low pH, with results correlating well with the MD simulations.

Stability of recombinant empty capsids

For empty particles the RNA fluorescence assay could not be used, so analysis was by fractionation on sucrose density gradients followed by western blot. Purified wild-type and mutant (S93H, S93Y and S93F) O1M capsids were heated at 45°C for 1h. The mutant empty capsids then sedimented similarly to intact particles, whilst wild-type empty capsid material stayed near the top of the gradient, confirming dissociation (Figure 2c and Supplementary Figure 3). In a more extreme test the mutant capsids were incubated at 56°C for 2h before analysis. Mutant S93H was unstable, S93Y partially stable (~25% dissociated particles as estimated by eye) and S93F completely stable. When visualized by EM, the peak fraction of heat-treated S93F revealed mostly intact capsids, with few pentamers (Supplementary Figure 4). Similar results were obtained with A22 empty capsids: the H93F mutant remained intact after 2h at 56°C, whereas wild-type capsids completely dissociated (Supplementary Figure 5). To study the effect of storage at moderate temperature on empty capsids, O1M wild-type and S93F mutant were incubated for 24h or 96h at 37°C. Wild-type capsids dissociated, whereas S93F capsids remained intact (Supplementary Figure 6). To determine pH stability, O1M capsids were incubated at pH 5.5 for 15 min. Wild-type capsids dissociated completely whereas S93H and S93Y capsids were partially stable (25% remained intact) and S93F remained completely intact (Figure 2c).

Structure analysis of stabilised capsids

We determined structures of the stabilised capsids by X-ray crystallography and cryo-EM. SAT2 crystals did not diffract to high resolution, however structures of the mutant A22 empty capsid and mutant O1M virus were solved at 2.4Å and 3.5Å resolution, respectively, using *in situ* room temperature X-ray crystallography17, 31. The O1M crystals were

merohedrally twinned and a protocol was developed to de-convolute the twinned reflections32 (HMG, unpublished). Refinement using strict non-crystallographic symmetry and real-space averaging gave reliable maps and models for both structures (Table 2). The refined atomic models were very similar to those of the respective natural empty particles and parental viruses10–12, 17, except that, as predicted the aromatic side chains of VP2 residue 93 stacked at the 2-fold axes. Due to the reduced quality of the O1M analysis, and the fact that we were unable to obtain diffraction quality crystals of SAT2 particles, we determined the structures of inactivated O1M S93Y and SAT2 S93Y by cryo-EM (Methods). 8,267 particles of O1M and 8,156 particles of SAT2 yielded structures at 3.2 and 3.5Å (FSC 0.143) resolution, respectively (Figure 3a and 3b, Supplementary Figure 7, Supplementary Table 3). The predicted and experimental stacking of the tyrosine and pheyalanine side chains around the 2-fold axis, from X-ray and CryoEM structures, are shown in (Figure 3c - e).

Immunogenicity of stabilised mutants

To compare the immunogenicity of wild-type and stabilised viruses, we vaccinated calves with purified inactivated wild-type or mutant (S93Y) virus of both the O1M and SAT2 serotypes. Inactivated antigen was maintained at 4°C and purified immediately prior to use. We measured Serum virus neutralisation antibody titre (VNT) at different times post-vaccination (pv) (Figure 4a). In all animals, high VNT were observed on day 28 at the time of boost immunisation, with mean antibody titres >2 $\log_{10}$, which is considered protective33 and titres were significantly increased (>3 $\log_{10}$) by day 42 pv.

As mutant and wild-type antigen had equivalent immunogenic properties when administered directly after purification, we compared their immunogenicity after long-term storage. For this, inactivated wild-type and mutant S93Y FMDV SAT2 particles at doses of 10μg each formulated as described above were stored for 1 month at 4°C and used to vaccinate two groups of ten guinea pigs. VNTs were assessed at three and six months post vaccination (pv) (Figure 4b). Three months pv, substantially higher VNTs were observed in animals vaccinated with the stabilised SAT2 antigen (>8 $\log_2$ considered protective34) when compared with those animals vaccinated with the wild-type SAT2 antigen (<3 $\log_2$). Six months pv, the group mean VNT in animals immunised with the stabilised SAT2 antigen remained at >8 $\log_2$, whilst wild-type immunized animals' antibody titres remained below protective levels. Thus, the stabilised vaccine performed markedly better than the wild-type vaccine.

In a further iteration, equivalent aliquots of wild-type and stabilised vaccines were stored for six months at 4°C and again used to immunise two groups of ten guinea pigs. No animal had a VNT titre at day 0 but by day 30 pv, while the mean VNT titre of the group inoculated with wild-type vaccine remained low (~3 $\log_2$), the mean titre of the group inoculated with stabilised virus was markedly higher and consistent with protection, >6 $\log_2$ (Figure 4c). Thus only stabilised particles were able to induce VNT titres consistent with protection after 1 month or 6 months storage at 4°C.

Discussion

More stable FMDV vaccines have the potential to be more effective. However, very few natural FMDV variants with increased resistance to heat or pH35, 36 have been reported, possibly because over-stabilisation hinders the release of the viral genome during cell entry. We have therefore investigated the rational introduction of mutations to increase thermo-stability, earlier attempts at which have had only marginal success16. We previously reported a stable disulphide bond at the icosahedral 2-fold axis between adjacent pentamers for the A22 virus, allowing the production of thermo- and pH stable recombinant empty particles17. Since covalent modification was unlikely to be suitable with engineered viruses and may not be generally applicable, we have devised a strategy that allows general mutations conferring non-covalent stabilisation to be evaluated *in silico*. We exploit highly restrained atomistic MD simulations focussed on the appropriate part of the complete virion to efficiently and reliably calculate the binding free energy for interactions between adjacent pentamers within the FMDV capsid, allowing screening and ranking of candidate mutations. We find that a single residue mutation generating hydrophobic stacking of aromatic side chains at the 2-fold axis between adjacent pentamers (position 93 of VP2) is effective in stabilising the particle, echoing enteroviruses where the particle opens up at this point to start uncoating20, 21. The predicted degree of stabilisation correlates with hydrophobicity, thus with O1M: S93H ($\Delta\Delta G$ = -7.7 kcal/mol) < S93Y ($\Delta\Delta G$ = -11.8 kcal/mol) < S93F ($\Delta\Delta G$ = -13.8 kcal/mol). Similarly, when the equivalent (histidine) residue of the stable A-serotype, A22 Iraq, is substituted by tyrosine ($\Delta\Delta G$ = -7.7 kcal/mol) or phenylalanine ($\Delta\Delta G$= -10.3 kcal/mol), the stability of the interface is further increased.

Engineering the stabilisation mutations reduced the plaque sizes for both O1M and SAT2 viruses, possibly by delaying viral genome release. Both infectious viruses and recombinant empty capsids carrying these mutations were indeed thermo- and pH-stable, with the degree of stabilisation mirroring the *in silico* calculations. This non-covalent stabilisation of two particularly unstable serotypes produced particles of similar stability to covalently cross-linked A22 particles17. Formulated vaccines from inactivated wild-type and stabilised O and SAT2 viruses, produced equivalent protective levels of neutralising antibodies in cattle, demonstrating the immunogenicity of the engineered particles. The stabilised inactivated vaccine antigen is also intact after 96 hours at 37°C and will be more tolerant of less than optimal cold chain performance; goals for the stability of SAT2 are given by Anderson et al. 37. Furthermore, after storage for one or six months at 4°C, stabilised particles produced substantially higher VNT in guinea pigs than wild-type, commensurate with an increase in vaccine shelf-life.

In conclusion, we have devised a novel restrained MD protocol to drive structure-based design of stabilised FMDV viruses and empty capsids. Such novel effective FMDV vaccines would, in the context of empty capsids, eliminate the considerable risks involved in producing vaccine from infectious virus. This strategy may be relevant to many other picornaviruses that are responsible for causing a wide range of mild to life threatening diseases affecting both humans and animals.

Online Methods

Molecular dynamics methods

These are described in the accompanying Supplementary Note.

Generation of infectious recombinant cDNA

Infectious FMDV O1K/O1Manisa (O1M) chimeric clones were constructed using reverse genetics. Briefly, cDNA encoding the VP2, VP3, VP1 and 2A proteins was removed from a derivative of the pT7S3 O1K infectious clone, termed pT7SBmuts, leaving cDNA encoding the Lpro, VP4, 2B, 2C, 3A, 3B, 3C and 3D proteins41. The removed cDNA was replaced with the corresponding O1M cDNA from pGEM9zf subclones, encoding the wild-type or a specific amino acid substitution within the VP2 structural protein42 (UKG/35/2001; GenBank accession no. AJ539141). The encoded amino acid substitutions within VP2 were generated using the QuikChange Lightning Mutagenesis kit (Agilent Technologies) according to the manufacturer's instructions. For SAT2, the leader-P1-2A coding region of pSAT243 was cloned into pBS (Stratagene) using *Eco*RI and *Xma*I restriction enzyme sites. Site-directed mutagenesis was performed according to QuikChange™ Site-Directed Mutagenesis Kit (Stratagene). The pSAT2/pBS clones containing the desired mutations, as verified by nucleotide sequencing, were digested with *Ssp*I and *Xma*I to recover the mutant leader-P1-2A region, which was cloned back into the pSAT2 genetic backbone. All mutations were verified by sequencing.

Preparation of infectious RNA, electroporation and transfection

RNA was transcribed from the infectious clones using the MEGAscript T7 kit (Invitrogen). Infectious RNA was electroporated using a Bio-Rad Gene PulsarTM (two pulses at 0.75 kV and 25 mF) or transfected into BHK-21 cells (clone 13). After 24 h, the cells were frozen then thawed in their growth media. Following clarification by centrifugation, the supernatant containing the initial virus stock (termed 'passage 0', P0) was harvested. Foetal goat tongue (ZZ-R 127) or BHK-21 cells were subsequently used to passage the viruses 44. Cells were infected for 24 h between passages. The yields of wild-type and mutant viruses were similar. BHK-21 cells (clone 13) have been maintained in the Pirbright institute since 1965. ZZ_R 127 cells were a gift from Bernd Haas Friedrich-Loeffler-Institut, (FLI) Greifswald, Germany. All cell cultures were free of mycoplasma and bovine viral diarrhea virus.

Genome amplification and sequencing

Total RNA was extracted using TRIzol (Invitrogen) and the viral RNA genome reverse transcribed and PCR amplified using a One-Step RT-PCR kit (Qiagen). Sequencing reactions were performed using an aliquot of the purified PCR product and the BIG Dye Terminator v3.1 cycle sequencing kit (Applied Biosystems).

Plaque assay

Confluent monolayers of goat epithelium or BHK-21 cells were infected with serial dilutions of virus stocks, overlaid with indubiose (Pall Life Sciences, France) and incubated for 24-48 h at 37°C. Cells were fixed and stained (4% formaldehyde in phosphate buffered

saline (PBS) containing methylene blue), and the overlay removed26. The diameters of 50 parental (wild-type) plaques were measured with a microscope eyepiece micrometer. These were averaged, defined as 100%, and compared against 50 mutant plaque diameters.

Virus Titres

Virus titres were estimated by plaque assays. For O1M, Confluent monolayers of BHK-21 cells were infected with serial dilutions of FMDV virus stocks in triplicate, overlaid with indubiose and incubated for 24 to 48 h at 37 °C. The cells were then fixed and stained (4% formaldehyde in PBS containing methylene blue) before removal of the overlay26. For SAT2, BHK-21 cells were infected for 1 h, followed by the addition of 2 ml tragacanth overlay45. Following incubation at 37ºC for 48 h the infected monolayers were stained with 1% (w/v) methylene blue in 10% (v/v) ethanol and 10% (v/v) formaldehyde in phosphate buffered saline, pH 7.4.

Virus Inactivation

Chemical inactivation followed standard operating procedures (SOPs) in-line with disease security regulations at The Pirbright Institute. Upon CPE, the cell culture medium, containing the virus, was harvested and clarified by centrifugation at 2,095 × g for 30 min at 4°C. Clarified supernatant was inactivated by two consecutive incubations with BEI (binary ethyleneimine). A 10 ml aliquot of 0.1M BEI solution was added to every 1000 ml of virus harvested (to give a final BEI concentration of 0.001 M) followed by incubation for 24 h at 37°C. During incubation, the virus/BEI solutions were mixed by periodic inversion. Innocuity tests were performed by the World Reference Laboratory (WRL) at The Pirbright Institute.

Generation of recombinant empty particles

Expression of recombinant empty capsids used two different systems: O1M capsids were produced using a vaccinia virus (VV) mammalian cell expression system and A22 capsids were produced using a baculovirus (BV) insect cell expression system according to reference 17. Briefly, for VV expression cassettes containing synthetic cDNA encoding VP0, VP3 and VP1 and the 2A and 3C non-structural proteins of wild-type FMDV were synthesized (GeneArt) and cloned into a VV vector, pBG200. Recombinant viruses were made by transfecting the pBG200 vector into simian kidney derived CV-1 cells that had been infected with VV. Recombinant VVs (VV-FMDV) were selected by plaque assay and verified by PCR using FMDV specific primers. FMDV empty capsids were amplified in RK13 or HEK293 cells following dual infection with a recombinant VV expressing T7 polymerase (VV-T7) as described17. For insect cell expression, pTri-EX-derived plasmid pOPINE46 was used to generate recombinant BVs encoding the FMDV proteins. The pOPINE vector containing the FMDV coding sequence, and the AcMNPV (Autographa californica nucleopolyhedrovirus) FlashBacGold DNA (from Oxford Expression Technologies), were transfected into *Sf9* insect cells (*Spodoptera frugiperda*) using Lipofectin. Recombinant AcMNPV was harvested from supernatant five days post infection (P0 virus stock) and amplified by infecting *Sf9* cells at 50% confluency with 200 μl recombinant virus per 175 cm^2 flask and collecting the supernatant after five days (P1 virus stock). Recombinant empty capsids were expressed by infecting *Sf9* cells (1-2 × 10^6/ml)

with 1/10 volume of the P1 BV stock. Mutants were made by PCR mutagenesis (QuikChange Lightning Mutagenesis Kit, Agilent technologies,) according to the manufacturer's instructions. CV-1, RK13 and HEK 293 cells were sourced from the European Collection of Cell Cultures (ECACC). All cell cultures were free of mycoplasma and bovine viral diarrhea virus. *Sf9* insect cells were sourced from Sigma Aldrich (UK).

Purification of viruses

Frozen lysates containing inactivated antigens were thawed on ice and clarified by centrifugation at 3,500 × g for 30 min at 4°C. Virus was then precipitated by the addition of either 30% w/v ammonium sulphate or 8% w/v polyethylene glycol 6000 (PEG6000) by incubation at 4°C overnight. Precipitated virus was harvested by centrifugation at 3,500 × g for 1 h at 4°C and re-suspended in 50 mM HEPES (4-(2-hydroxyethyl)-1-piperazineethanesulfonic acid), pH 7.5 containing 200 mM NaCl and 1% v/v NP40, treated with 0.1% RNase-A for 30 min on ice and again clarified by centrifugation at 3,500 × g for 1 h at 4°C to remove insoluble particulates. Capsids were pelleted over a 3 ml, 30% sucrose cushion (in 50 mM HEPES, pH 7.5 containing 200 mM NaCl) at 105,000 × g for 2.5 h at 4°C. Pellets were re-suspended in HEPES buffer containing 0.5% (v/v) NP40 overnight at 4°C, clarified by centrifugation (16,000 × g for 10 min at 4°C) and purified over a 15-45% sucrose gradient. The gradient was layered with the clarified supernatant containing virus and fractionated by centrifugation at 105,000 × g for 3 h at 4°C. Fractions were analysed by SDS-PAGE followed by Coomassie staining.

Purification of recombinant empty capsids

Mammalian cells dually infected with VV-FMDV and VV-T7 were harvested by centrifugation at 3,500 × g for 30 min at 4°C and pellets re-suspended in PBS. Frozen recombinant BV infected *Sf9* cell pellets containing over-expressed empty capsids were thawed and re-suspended in 50 mM HEPES pH 7.5, 200 mM NaCl and 1% NP40. Cells were lysed by incubating with detergent for 30 min on ice. Lysates were clarified at 10,000 × g for 30 min at 4°C and capsids pelleted over a 3 ml, 30% sucrose cushion by centrifugation at 105,000 × g for 5 h at 12°C. Thereafter recombinant capsids were purified as described for inactivated virus and analysed by SDS-PAGE followed by Coomassie staining.

Negative stain electron microscopy

Aliquots of purified samples were diluted to 0.2 mg/ml and deposited onto glow-discharged, Formvar/carbon-coated copper grids (Electron Microscopy Sciences, P.O. Box 550, 1560 Industry Road, Hatfield, US). After 30 seconds incubation, the excess sample was blotted away and the grids washed twice with deionized water. Samples were stained with 1% (w/v) uranyl acetate for 45 seconds and excess stain was removed by blotting. Grids were examined on a Tecnai T12 transmission electron microscope operated at 80kV. Images were acquired on a 4k x 4k High-sensitivity FEI Eagle camera at 67000X magnification which corresponded to 1.68 Å/pix sampling of the specimen.

Thermo- and pH-stability assay for particles

The particle stability thermal release assay (PaSTRy)29 was performed in 96-well PCR plates using an Agilent MX3005 PCR machine. All assays were performed using 300-500 ng of purified virus (3-15 μl) that had been dialysed to remove most of the sucrose from purification. 15 μl of SYBR Green-II dye (Molecular Probes, Invitrogen) diluted 1:100 in the same buffer as used for virus purification and the volume made up to 150 μl with buffer. The temperature was ramped from 25°C to 95°C in 0.5°C increments with intervals of 10 s. SYBR Green-II fluorescence was read with excitation and emission wavelengths of 490 nm and 516 nm, respectively. The release of RNA and hence the dissociation of capsids was detected by an increase in fluorescence signal and the melting temperature was taken as the minimum of the negative first derivative of the fluorescence curve.

ELISA assay

Wild-type or S93Y particles were incubated at 37°C for up to 72 h and their stability was analysed by double antibody sandwich ELISA using llama single-domain antibody fragments ((VHH domains), termed VHH M170 that binds intact FMD viral particles and VHH M3 that recognises pentamer subunits). VHHs were provided by the Central Veterinary Institute of Wageningen UR, AB Lelystad, The Netherlands30. Microtitre plate wells were coated with VHHs before the addition of serially diluted samples (in VHH buffer: 1% skimmed milk; 0.05% Tween; 0.5M NaCl; 2.7mM KCl; 2.8mM KH2PO4; 8.1mM Na2HPO4, pH 7.4.). Following incubation for 1 hour at 37°C, biotinylated VHH M170 was then added and incubated for a further 1 hour at 37°C. Plates were washed with PBS-Tween (0.05% Tween 20) and bound biotinylated VHH-M170F was visualised by incubation with streptavidin-HRP (Dako, UK) for 1 hr at 37°C followed by addition of o-phenylenediamine dihydrochloride (Sigma, UK) for 15 minutes at room temperature. The reaction was stopped by addition of 1.25M sulphuric acid and quantified at 492nm using a Dynex microplate reader (Dynex Technologies, UK).

Stability assay for recombinant empty capsids

Sucrose gradient purified samples of FMDV empty capsids were diluted with PBS and incubated in a water bath at either 45°C for 1 h or 56°C for 2 h. They were then loaded onto 15-45% sucrose density gradients and sedimented. The gradients were fractionated from the bottom to the top and an equal volume of saturated ammonium sulphate was added to 300 μl of each fraction in order to precipitate any empty capsids present. Pelleted precipitates were analysed by SDS PAGE and western blot for the VP1 capsid protein, using guinea-pig polyclonal anti-sera (Supplementary Figure 3). In similar experiments, samples containing empty capsids were diluted with 50 mM sodium acetate buffer pH 4.6 to give a pH range of 5.5 to 6.5 (in 0.5 unit increments) and incubated for 15 min at room temperature. After neutralization with 1/6 volume of 2 M NaOH47, the empty capsids were loaded onto 15-45% sucrose density gradients, and treated as described above before analysis by SDS PAGE and western blot.

Crystallisation, data collection and structure determination

Crystals were grown by the sitting-drop vapour diffusion method in Crystalquick X plates (Greiner Bio-One) using 100 nl virus/empty capsids plus 100 nl precipitant dispensed with a Cartesian robot as described previously48. Micro-crystals of inactivated O1M S93Y virus (2.2 mg/ml) and A22 H93F empty capsids (3 mg/ml) grew within 1 week at 294K with 1.5 M ammonium sulphate, 100 mM bis-Tris Propane, pH 7.0 and 4 M ammonium acetate, 100 mM bis-Tris Propane, pH 7.0 respectively. Optimisation produced sufficient crystals for structural solution. A 20 × 20 μm^2 or 50 × 50 μm^2 beam (λ = 0.9778 Å; I24 micro-focus beamline, Diamond), depending on the crystal size, was used for *in situ*31 data collection at 294 K on a Pilatus 6 M detector.

The structures of O1M S93Y and A22 H93F were solved by molecular replacement using the co-ordinates and non-crystallographic symmetry (NCS) operators from O1BFS (PDB ID: 1BBT)22 and A22 (PDB ID: 4GH4)11. Initial phase estimates were obtained by rigid body refinement with CNS49. Twinned data sets were de-convoluted by combining five-fold NCS averaging in real space with rescaling individual reflections according to the twinning operator. This uses redundancy of information in the NCS to recover information lost by the superimposed 90° rotation twinning operation. Iterative positional and B-factor refinement (via CNS) used strict NCS constraints. Phases were further improved by 15-fold (A22) and 5-fold (O1M) NCS averaging. The percentage of Ramachandran outliers was 0 and 16.7 for A22 and O1M structures, respectively.

Cryo-EM data collection, structure determination and model building

Aliquots of 4 μl of purified inactivated O1M or SAT2 mutant S93Y virus were added on glow-discharged holey carbon-coated copper grids (C-flat, CF-2/1-2C; Protochips Inc.). Grids were blotted for 3s, in 70% relative humidity, and vitrified in liquid ethane using a plunger device (Vitrobot; FEI, Hilsboro, OR). To increase the number of particles in the holes, grids were pre-incubated with 4 μl of sample for 30 s and unbound sample was removed by blotting with filter paper.

Images were collected at 300kV using a Tecnai F30 ‘Polara’ microscope (FEI, Hillsboro, OR) equipped with an energy filter (GIF Quantum; Gatan, Pleasanton, CA) operating in zero-loss mode (0–20 eV energy selecting slit) and a direct electron detector (K2 Summit; Gatan, Pleasanton, CA). Movies (25 frames, each 0.2 s) were recorded at 1.0–3.0 μm underfocus in single electron counting mode using SerialEM at a calibrated magnification of 37,027×, resulting in a pixel size of 1.35 Å. Frames from each movie were aligned and averaged to produce drift corrected micrographs50.

Structures were solved using RELION 1.3 following recommended gold-standard refinement procedures51 and applying icosahedral symmetry. Micrographs showing signs of astigmatism or significant drift were discarded and not used for further analysis. Reference free 2D class averaging was used to discard bad particles. Particle population was further improved by 3D classification. The X-ray structure of native FMDV A22 serotype (PDB ID: 4GH4)11 was low pass-filtered to 50 Å and used as an initial template for 3D classification and refinement. A total of 8267 O1M particles from 210 micrographs and 8156 SAT2

particles from 321 micrographs were used to solve the final density maps at 3.2Å and 3.5Å resolution, respectively, as indicated by Fourier shell correlation and 0.143 cut-off (Supplementary Figure 7). The O1M mutant was fitted in the density map as a rigid-body using UCSF Chimera52. The fitting was further improved using real space refinement using COOT23. The model of SAT2 was built using the SAT1 structure as a starting model using COOT23. REFMAC53 was used to calculate the difference map which highlighted the areas where the model was incorrect. Models were further improved by iterative positional and B-factor refinement in real space using Phenix54 and COOT23 iteratively. Only coordinates were refined, the maps were kept constant. Each round of model optimization was guided by cross-correlation between the map and the model. Statistics of refinement are given in Supplementary Table 3.

Cattle and guinea pigs vaccination with stabilised FMDV vaccines

Four groups of four 100 to 150 kg male Holstein Friesian calves were vaccinated with either inactivated: O1M-wt, O1M-(S93Y), SAT2-wt or SAT2-(S93Y) FMDV. Each animal received 15 μg of purified 146S antigen formulated in oil adjuvant ISA206B (SEPPIC) as an intramuscular injection on days 0 and 28 of the study. All sixteen animals were bled to collect serum on days 0, 28, 35 and 42 and virus neutralising antibody titres (VNT) were assessed. Animal experimentation was approved by the Pirbright Institute Ethical Review Board under the authority of a Home Office project licence (70/7253) in accordance with the Home Office Guidance on the Operation of the Animals (Scientific Procedures) Act 1986 and associated guidelines.

For the guinea pig experiments inactivated SAT2 wild-type and stabilised mutant S93Y were formulated as commercial vaccines using oil-based ISA206B (SEPPIC) adjuvant and stored for 1 month at 4°C. Aliquots containing 10 μg of 146S antigen at the time of formulation of these vaccines were then used to immunise two groups of 10 adult inbred Guinea pigs, age 2-4 months. One group received the wild-type vaccine while the other group received the stabilised vaccine. Serum samples were tested on day 0, followed by 3 and 6 months pv bleeds and virus VNT were assessed. The experiments were repeated using the same volumes after the vaccines had been stored for a total of 6 months at 4°C. Serum samples were collected on days 0 and 30 pv and the VNTs analysed. All studies in the Netherlands complied with the Dutch Experiments on Animals Act, February 5, 1997. All studies complied with the Council Directive 86/609/EEC on the approximation of laws, regulations and administrative provisions of the Member States regarding the protection of animals used for experimental and other scientific purposes.

No statistical method was used to predetermine sample size. Group sizes for the cattle and guinea pig immunisation studies were consistent with previous published studies used to determine the induction of antibody titres consistent with protection33, 34. No randomisation was performed. The laboratory staff performing the assessment of antibody titres were not aware of the animal group allocations.

Titration of neutralising antibodies

Sera from guinea pigs and cattle were prepared from blood samples. Sera obtained at weekly intervals from day 0 to day 42 pv were assayed by a standard VNT test (OIE, 2012) on porcine kidney IB-RS2 cells using O1Manisa and SAT2 wild-type viruses. Neutralizing antibody titres, calculated by the Spearmann-Karber method, were expressed as the last dilution of serum that neutralizes 50% of the homologous virus (100TCID50)44. The mean antibody titres of each group of animals was compared with threshold antibody titres that have been shown previously to correlate with protection33, 34.

Supplementary Material

Refer to Web version on PubMed Central for supplementary material.

Acknowledgements

We thank the WRL for VNT determination, beamline staff at Diamond Light Source for assistance. J. Dong and J. Diprose for IT support, P. Afonine and G. Murshudov for advice on Phenix and Refmac, K. Harlos and T. Walter for help on crystallography and D. Goovaerts and E. Rieder for helpful discussions. We are grateful to the Wellcome Trust for a translation award to fund this work (grant no 089755, to B.C., E.E.F., T.J., D.I.S. and F.M.). The OPIC electron microscopy facility was founded by a Wellcome Trust JIF award (060208/Z/00/Z to D.I.S.) and is supported by a WT equipment grant (093305/Z/10/Z to Kay Gruenwald). The Wellcome Trust, UK Medical Research Council (MRC) and Biotechnology and Biology Research Council also support the National EM facility, which enabled provision of the K2 detector. B.C. and D.I.S. are supported as Jenner investigators, J.R. and A.K. are Wellcome Trust-supported and E.E.F. and D.I.S. are supported by the UK MRC (grant no G100099 to D.I.S.). The work of the Wellcome Trust Centre in Oxford is supported by the Wellcome Trust core award 090532/Z/09/Z.

References

1. Grubman MJ, Baxt B. Foot-and-mouth disease. Clin Microbiol Rev. 2004; 17:465–493. [PubMed: 15084510]
2. Muroga N, et al. The 2010 foot-and-mouth disease epidemic in Japan. J Vet Med Sci. 2012; 74:399–404. [PubMed: 22075710]
3. Kandeil A, et al. Characterization of the recent outbreak of foot-and-mouth disease virus serotype SAT2 in Egypt. Archives of Virology. 2013; 158:619–627. [PubMed: 23132412]
4. Bachrach HL. Foot-and-mouth disease. Annu Rev Microbiol. 1968; 22:201–244. [PubMed: 4301615]
5. Doel TR. FMD vaccines. Virus Res. 2003; 91:81–99. [PubMed: 12527439]
6. Doel TR, Baccarini PJ. Thermal stability of foot-and-mouth disease virus. Arch Virol. 1981; 70:21–32. [PubMed: 6277281]
7. Doel TR, Chong WKT. Comparative immunogenicity of 146S, 75S and 12S particles of foot-and-mouth disease virus. Archives of Virology. 1982; 73:185–191. [PubMed: 6293410]
8. Hall MD, Knowles NJ, Wadsworth J, Rambaut A, Woolhouse MEJ. Reconstructing Geographical Movements and Host Species Transitions of Foot-and-Mouth Disease Virus Serotype SAT 2. mBio. 2013; 4
9. Basavappa R, et al. Role and mechanism of the maturation cleavage of VP0 in poliovirus assembly: Structure of the empty capsid assembly intermediate at 2.9 Å resolution. Protein Science. 1994; 3:1651–1669. [PubMed: 7849583]
10. Acharya R, et al. The three-dimensional structure of foot-and-mouth disease virus at 2.9 A resolution. Nature. 1989; 337:709–716. [PubMed: 2537470]
11. Curry S, et al. Perturbations in the surface structure of A22 Iraq foot-and-mouth disease virus accompanying coupled changes in host cell specificity and antigenicity. Structure. 1996; 4:135–145. [PubMed: 8805520]

12. Curry S, et al. Dissecting the roles of VP0 cleavage and RNA packaging in picornavirus capsid stabilization: the structure of empty capsids of foot-and-mouth disease virus. J Virol. 1997; 71:9743–9752. [PubMed: 9371640]
13. Lea S, et al. The structure and antigenicity of a type C foot-and-mouth disease virus. Structure. 1994; 2:123–139. [PubMed: 8081743]
14. Reeve R, et al. Sequence-Based Prediction for Vaccine Strain Selection and Identification of Antigenic Variability in Foot-and-Mouth Disease Virus. PLoS Comput Biol. 2010; 6:e1001027. [PubMed: 21151576]
15. Ellard FM, Drew J, Blakemore WE, Stuart DI, King AM. Evidence for the role of His-142 of protein 1C in the acid-induced disassembly of foot-and-mouth disease virus capsids. J Gen Virol. 1999; 80:1911–1918. [PubMed: 10466786]
16. Mateo R, Luna E, Rincón V, Mateu MG. Engineering Viable Foot-and-Mouth Disease Viruses with Increased Thermostability as a Step in the Development of Improved Vaccines. Journal of Virology. 2008; 82:12232–12240. [PubMed: 18829763]
17. Porta C, et al. Rational Engineering of Recombinant Picornavirus Capsids to Produce Safe, Protective Vaccine Antigen. PLoS Pathog. 2013; 9:e1003255. [PubMed: 23544011]
18. Berman HM, et al. The Protein Data Bank. Nucleic Acids Research. 2000; 28:235–242. [PubMed: 10592235]
19. Wang X, et al. A sensor-adaptor mechanism for enterovirus uncoating from structures of EV71. Nat Struct Mol Biol. 2012; 19:424–429. [PubMed: 22388738]
20. Ren J, et al. Picornavirus uncoating intermediate captured in atomic detail. Nat Commun. 2013; 4
21. Butan C, Filman DJ, Hogle JM. Cryo-electron microscopy reconstruction shows poliovirus 135S particles poised for membrane interaction and RNA release. J Virol. 2014; 88:1758–1770. [PubMed: 24257617]
22. Fry E, Acharya R, Stuart D. Methods used in the structure determination of foot-and-mouth disease virus. Acta Crystallogr A. 1993; 49:45–55. [PubMed: 8382928]
23. Emsley P, Cowtan K. Coot: model-building tools for molecular graphics. Acta Crystallographica Section D. 2004; 60:2126–2132.
24. Karplus M, McCammon JA. Molecular dynamics simulations of biomolecules. Nat Struct Biol. 2002; 9:646–652. [PubMed: 12198485]
25. Klepeis JL, Lindorff-Larsen K, Dror RO, Shaw DE. Long-timescale molecular dynamics simulations of protein structure and function. Current Opinion in Structural Biology. 2009; 19:120–127. [PubMed: 19361980]
26. Jackson T, Sheppard D, Denyer M, Blakemore W, King AM. The epithelial integrin alphavbeta6 is a receptor for foot-and-mouth disease virus. J Virol. 2000; 74:4949–4956. [PubMed: 10799568]
27. Fry EE, et al. The structure and function of a foot-and-mouth disease virus-oligosaccharide receptor complex. Embo J. 1999; 18:543–554. [PubMed: 9927414]
28. Porta C, et al. Efficient production of foot-and-mouth disease virus empty capsids in insect cells following down regulation of 3C protease activity. J Virol Methods. 2013; 187:406–412. [PubMed: 23174161]
29. Walter TS, et al. A plate-based high-throughput assay for virus stability and vaccine formulation. J Virol Methods. 2012; 185:166–170. [PubMed: 22744000]
30. Harmsen MM, Fijten HP, Westra DF, Coco-Martin JM. Effect of thiomersal on dissociation of intact (146S) foot-and-mouth disease virions into 12S particles as assessed by novel ELISAs specific for either 146S or 12S particles. Vaccine. 2011; 29:2682–2690. [PubMed: 21316500]
31. Axford D, et al. In situ macromolecular crystallography using microbeams. Acta Crystallogr D Biol Crystallogr. 2012; 68:592–600. [PubMed: 22525757]
32. Lea S, Stuart D. Deconvolution of fully overlapped reflections from crystals of foot-and-mouth disease virus O1 G67. Acta Crystallogr D Biol Crystallogr. 1995; 51:160–167. [PubMed: 15299317]
33. Barnett PV, Statham RJ, Vosloo W, Haydon DT. Foot-and-mouth disease vaccine potency testing: determination and statistical validation of a model using a serological approach. Vaccine. 2003; 21:3240–3248. [PubMed: 12804854]

34. Bolwell C, Parry NR, Rowlands DJ. Comparison between in vitro neutralization titres and in vivo protection against homologous and heterologous challenge induced by vaccines prepared from two serologically distinct variants of foot-and-mouth disease virus, serotype A22. J Gen Virol. 1992; 73:727–731. [PubMed: 1312129]
35. Martin-Acebes MA, Rincon V, Armas-Portela R, Mateu MG, Sobrino F. A single amino acid substitution in the capsid of foot-and-mouth disease virus can increase acid lability and confer resistance to acid-dependent uncoating inhibition. J Virol. 2010; 84:2902–2912. [PubMed: 20053737]
36. Mateo R, Luna E, Mateu MG. Thermostable variants are not generally represented in foot-and-mouth disease virus quasispecies. J Gen Virol. 2007; 88:859–864. [PubMed: 17325358]
37. Anderson EC, Doughty WJ, Spooner PR. Variation in the thermal stability of isolates of foot-and-mouth disease type SAT 2 and its significance in the selection of vaccine strains. Journal of Comparative Pathology. 1982; 92:495–507. [PubMed: 6296205]
38. Tang G, et al. EMAN2: an extensible image processing suite for electron microscopy. J Struct Biol. 2007; 157:38–46. [PubMed: 16859925]
39. Ferris NP, et al. Utility of recombinant integrin alpha v beta6 as a capture reagent in immunoassays for the diagnosis of foot-and-mouth disease. J Virol Methods. 2005; 127:69–79. [PubMed: 15893568]
40. Ferris NP, Donaldson AI. Serological response of guinea pigs to inactivated 146S antigens of foot and mouth disease virus after single or repeated inoculations. Rev Sci Tech Off Int Epiz. 1984; 3:563–574.
41. Botner A, et al. Capsid proteins from field strains of foot-and-mouth disease virus confer a pathogenic phenotype in cattle on an attenuated, cell-culture-adapted virus. J Gen Virol. 2011; 92:1141–1151. [PubMed: 21270284]
42. Zibert A, Maass G, Strebel K, Falk MM, Beck E. Infectious foot-and-mouth disease virus derived from a cloned full-length cDNA. J Virol. 1990; 64:2467–2473. [PubMed: 2159523]
43. van Rensburg HG, Henry TM, Mason PW. Studies of genetically defined chimeras of a European type A virus and a South African Territories type 2 virus reveal growth determinants for foot-and-mouth disease virus. J Gen Virol. 2004; 85:61–68. [PubMed: 14718620]
44. Brehm KE, Ferris NP, Lenk M, Riebe R, Haas B. Highly sensitive fetal goat tongue cell line for detection and isolation of foot-and-mouth disease virus. J Clin Microbiol. 2009; 47:3156–3160. [PubMed: 19656987]
45. Rieder E, Bunch T, Brown F, Mason PW. Genetically engineered foot-and-mouth disease viruses with poly(C) tracts of two nucleotides are virulent in mice. J Virol. 1993; 67:5139–5145. [PubMed: 8394441]
46. Berrow NS, et al. A versatile ligation-independent cloning method suitable for high-throughput expression screening applications. Nucleic Acids Research. 2007; 35:e45. [PubMed: 17317681]
47. Curry S, et al. Viral RNA modulates the acid sensitivity of foot-and-mouth disease virus capsids. J Virol. 1995; 69:430–438. [PubMed: 7983739]
48. Walter TS, et al. A procedure for setting up high-throughput nanolitre crystallization experiments. Crystallization workflow for initial screening, automated storage, imaging and optimization. Acta Crystallogr D Biol Crystallogr. 2005; 61:651–657. [PubMed: 15930615]
49. Brunger AT, et al. Crystallography & NMR system: A new software suite for macromolecular structure determination. Acta Crystallogr D Biol Crystallogr. 1998; 54:905–921. [PubMed: 9757107]
50. Li X, et al. Electron counting and beam-induced motion correction enable near-atomic-resolution single-particle cryo-EM. Nat Meth. 2013; 10:584–590.
51. Scheres SHW. RELION: Implementation of a Bayesian approach to cryo-EM structure determination. Journal of Structural Biology. 2012; 180:519–530. [PubMed: 23000701]
52. Pettersen EF, et al. UCSF Chimera--a visualization system for exploratory research and analysis. J Comput Chem. 2004; 25:1605–1612. [PubMed: 15264254]
53. Murshudov GN, et al. REFMAC5 for the refinement of macromolecular crystal structures. Acta Crystallographica Section D. 2011; 67:355–367.

54. Wang Z, et al. An atomic model of brome mosaic virus using direct electron detection and real-space optimization. Nat Commun. 2014; 5

Europe PMC Funders Author Manuscripts

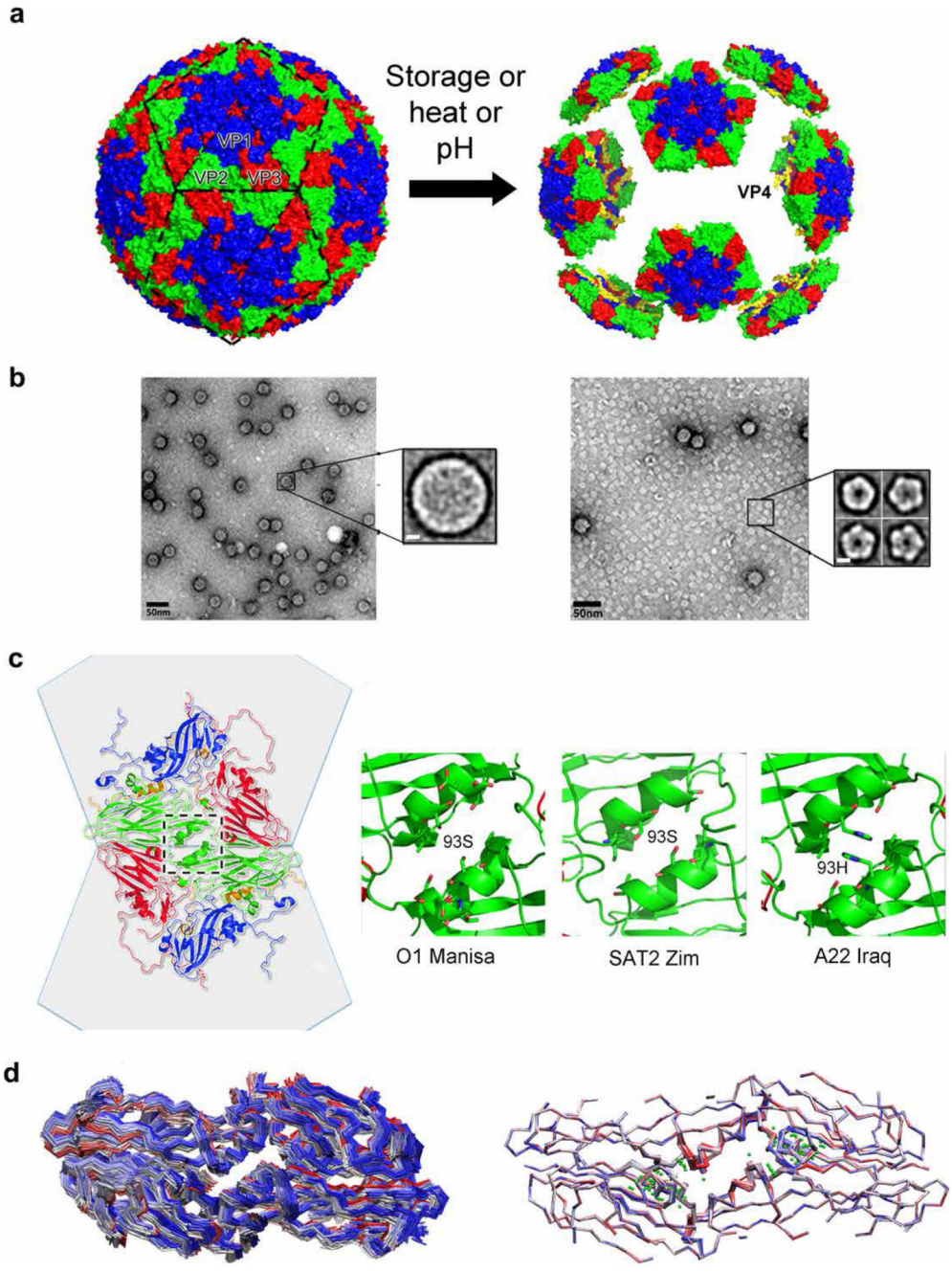

Figure 1. Dissociation of FMDV capsids into pentameric assemblies and design of the models used for MD simulations.

FMDV capsids readily fall apart into pentameric assemblies. (**a**) Surface representation of atomic models of the intact FMDV serotype O capsid (left panel; PDB 1BBT) and of its dissociation into twelve pentameric assemblies upon storage, heating or lowering pH (right panel). VP1, VP2, VP3 and VP4 are labelled and coloured blue, green, red and yellow, respectively. (**b**) Negative stain EM images of the inactivated O1M wild-type capsids soon after purification (left panel; intact with only a few detectable pentamers) or after 10 days of

storage at 4°C (right panel; 80% dissociated into pentamers). The scale bar indicates 50nm. Class averages of the intact capsid or pentamers are shown in the zoom windows (each calculated from 700 particles using EMAN238). The scale bar indicates 5nm. (**c**) Cartoon representation of the atomic structure of the O1M model showing two icosahedral protomers forming an inter-pentameric interface (left panel; VP1, VP2, VP3 and VP4 are labelled and coloured blue, green, red and yellow, respectively). A truncated model was generated by trimming the protomers to include VP2 and VP3 atoms within 13Å of the interface as shown in (**d**). Residues on 2-fold symmetry-related helices for O, A and SAT serotypes are highlighted in right panel. (**d**) 1.5ns MD trajectory showing a large RMSD from the starting structure for an unrestrained model (average RMSD 1.83 $Å^2$) in the left panel, with the restrained MD trajectory shown in the right panel (dummy atoms shown in green are placed at the midpoints of the inter-protomeric interface to define the restraints). The beginning of the trajectory is shown in red, the middle in white and the end in blue.

Europe PMC Funders Author Manuscripts

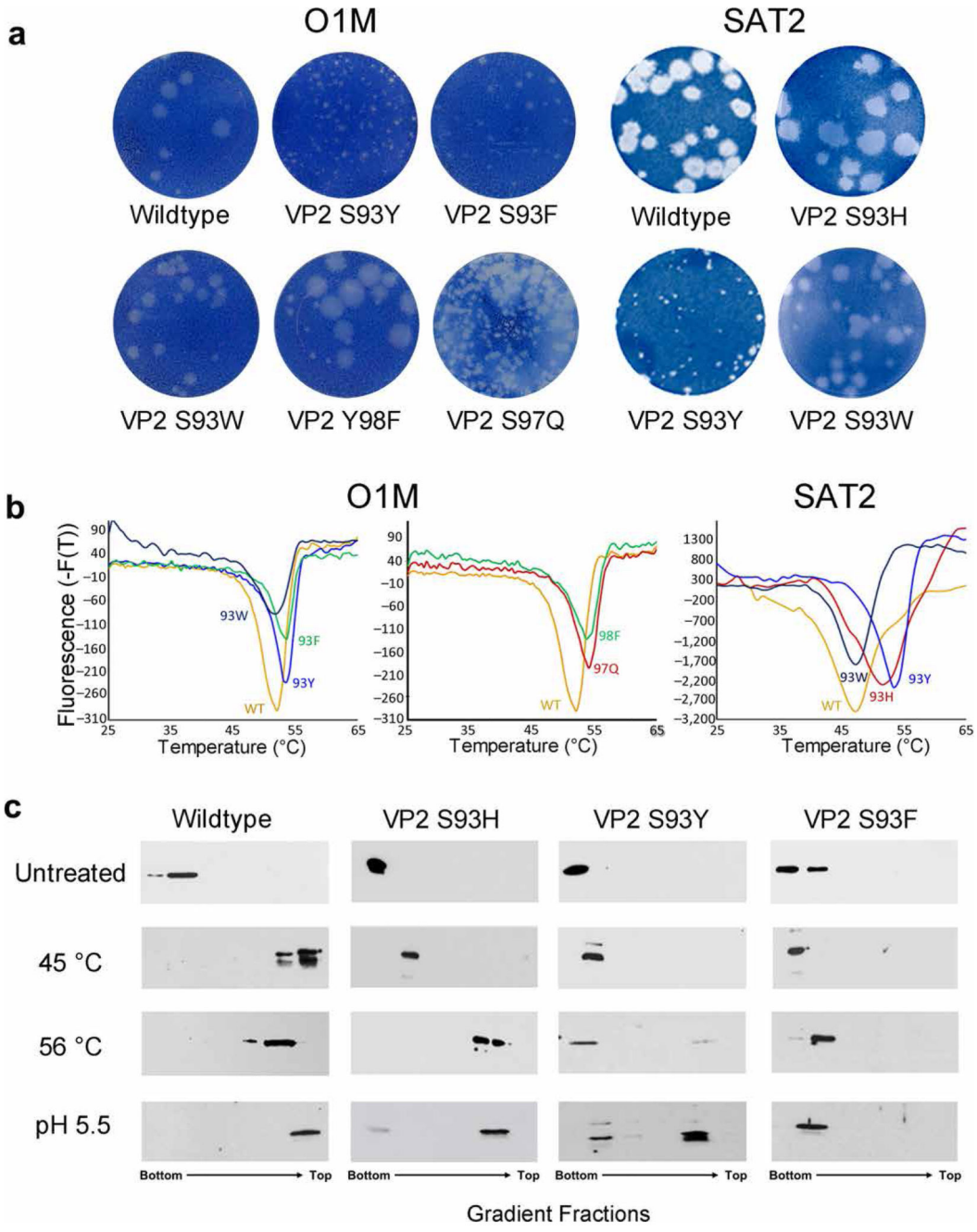

Figure 2. Growth characteristics and stability of the engineered capsids.

(**a**) Plaques formed in BHK-21 cells by wild-type and mutant O1M and SAT2 viruses. The patterns of CPE correlated with plaque size. (**b**) Fluorescence assay to measure thermostability of infectious O1M viruses (left and middle panels) and inactivated SAT2 viruses (right panel) at pH 7.5 29. Wild-type O1M and SAT2 dissociated at 52.0°C and 47.0°C, respectively. Mutant S93Y dissociated at 53.5°C for both O1M and SAT2. O1M mutants S93F, S97Q and Y98F dissociated at 53.5°C, 54.0°C and 53.5°C, respectively. Mutant S93H (SAT2) dissociated at 51.0°C. S93W was similar to that of parental virus in

both O1M and SAT2. (**c**) Thermo- and pH-stability of the recombinant empty capsids assayed by western blot after sedimentation through 15-45% sucrose density gradients. Dissociated capsids remain at the top of the gradient whereas intact capsids migrated near the bottom. Fractions were probed using anti-FMDV O1M polyclonal antibodies recognising VP139, 40 (see Supplementary Figure 3). Uncropped gels are shown in Supplementary Data Set 1.

Europe PMC Funders Author Manuscripts

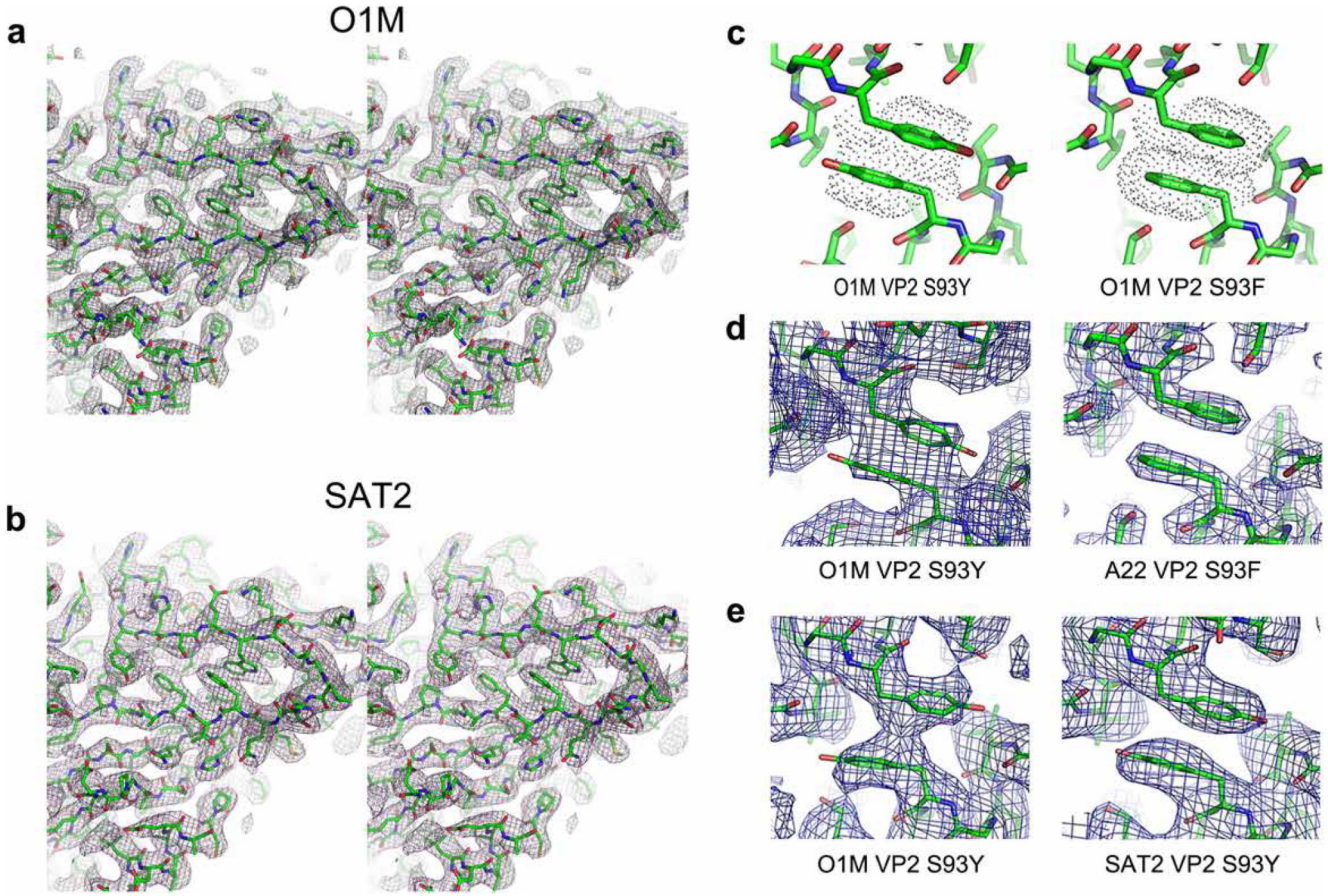

Figure 3. Structural analysis of stable engineered capsids.

The structures of engineered mutants O1M S93Y, A22 H93F and SAT2 S93Y were determined using X-ray crystallography and cryo-EM. (**a)** and (**b**) Stereo views of the density from cryo-EM reconstructions, the quality of the cryo-EM density maps allowed unambiguous fitting and refinement of the major capsid proteins for both (**a**) Cryo-EM structure of O1M S93Y at 3.2Å and (**b**) Cryo-EM structure of SAT2 S93Y at 3.5Å. (**c**) Predicted structures showing the stacking interactions of tyrosine and phenylalanine at position 93 of O1M VP2 proteins on the 2-fold symmetry axis. (**d**) X-ray structures of O1M S93Y and A22 H93F at 3.5Å and 2.4Å resolution, respectively. The electron-density map clearly showed a stacking interaction of phenylalanine side chains for A22 H93F. The tyrosine density for O1M S93Y was also observed but it was less well defined due to the twinning of O1M crystals. (**e**) Cryo-EM maps showing the density for S93Y for O1M and SAT2 at 3.2Å and 3.5Å resolution, respectively.

Europe PMC Funders Author Manuscripts

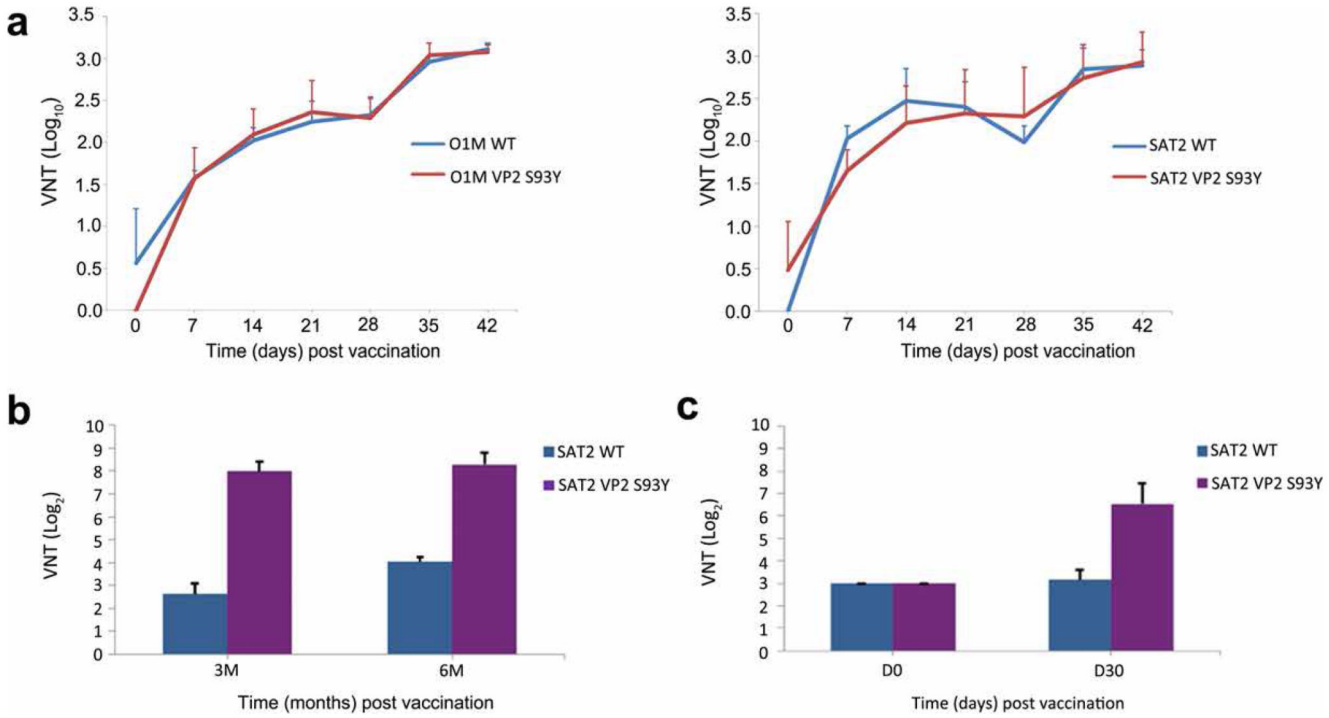

Figure 4. Immunogenicity of inactivated wild-type and stabilised viruses.

(**a**) Groups of four calves were vaccinated with purified inactivated virus of the O1M (left) and SAT2 (right) serotypes using in both cases either wild-type or mutant S93Y at days 0 and 28. The group mean virus neutralising antibody titre (VNT (log_{10})) are shown for blood samples assayed at 0, 7, 14, 21, 28, 35 and 42 days pv. Error bars represent the standard deviation. (**b**) Immunogenicity after long-term storage was assessed using inactivated wild-type and mutant S93Y FMDV SAT2 particles in a guinea pig trial. Two groups of 10 guinea pigs were each immunised with either mutant S93Y or wild-type SAT2 antigen. Prior to immunisation, formulated vaccines were stored for one month at 4°C. VNTs were assessed at three and six months pv. Error bars represent the standard deviation. (**c**) Equivalent aliquots of wild-type and stabilised SAT2 vaccines were stored for six months at 4°C prior to inoculation of two groups of ten guinea pigs. Only stabilised antigen shows evidence of protective VNTs. Error bars represent the standard deviation.

Europe PMC Funders Author Manuscripts

Europe PMC Funders Author Manuscripts

Table 1

Capsid stabilising mutants for O1M, SAT2 and A22.

A set of single amino acid substitutions at, or near the 2-fold axis, on the α-helix of the inter-pentamer interface is given in the top section. The change in binding free energy is calculated as described in Online Methods. Several mutants where found to be thermo- and pH- stable in three different serotypes of FMDV. A set of negative controls were also tested for O1M serotype to validate the simulation protocol. In one simulation VP2 arginine at position 60, that forms the salt bridge with the VP2 glutamate 212 on the opposite protomer, was substituted with either glycine or leucine; as expected, in both cases the interface was destabilised. Similarly, when glutamine at position 57, that makes a network of H-bonds across the interface, was substituted with glutamate or leucine an unstable interface was generated.

	O1-Manisa	**SAT2-Zim**	**A22-Iraq**
Mutation	**ΔΔG kcal/mol**	**ΔΔG kcal/mol**	**ΔΔG kcal/mol**
VP2 93H	- 7.7	-5.3	N/A
VP2 93Y	- 11.8	-12.2	-7.7
VP2 93F	- 13.8	-13.2	-10.3
VP2 98F	-10.3	-5.6	-
VP2 97I	- 6.8	-	-
VP2 93V	-7.1	-	-
VP2 93L	-1.9	-	-
VP2 93I	-7.2	-	-
VP2 93M	-2.8	-	-
VP2 93W	- 9.5	-	-
VP2 97Q	- 5.5	-	-
VP2 90N	- 3.5	-	-

Negative Controls	**O1-Manisa**
Mutation	**ΔΔG kcal/mol**
VP2 60G	+ 33.7
VP2 60L	+ 24.0
VP2 57E	+ 17.7
VP2 57L	+ 12.3

Table 2

Data collection and refinement statistics

	O1M VP2 S93Y[a]	A22 VP2 H93F[b]
Data collection		
Space group	I23	I222
Cell dimensions		
a, *b*, *c* (Å)	344.08, 344.08, 344.08	327.6, 341.3 363.6
α, β, γ (°)	90, 90, 90	90, 90, 90
Resolution (Å)	46.0 – 3.5 (3.56 – 3.5)[c]	50.0 – 2.4 (2.49 - 2.4)
R_{merge}	0.46	0.27
$I / \sigma I$	1.7(0.76)	1.23 (0.5)
Completeness (%)	77.7 (71.1)	45.5 (39.8)
Redundancy	1.5(1.4)	1.4 (1.3)
Refinement		
Resolution (Å)	46.0 – 3.5	50.0 – 2.4
No. reflections	65,915	347,924
R_{work} / R_{free}	36.35 / -	20.6/21.2
No. atoms		
Protein	5149	5192
Ligand/ion	-	-
Water	0	196
B factors		
Protein	49.2	27.0
Ligand/ion	-	-
Water	-	30.6
r.m.s. deviations		
Bond lengths (Å)	0.011	0.013
Bond angles (°)	1.816	1.716

[a] The data for O1M VP2 S93Y was collected from 14 different crystals

[b] The data for A22 VP2 H83F was collected from 19 different crystals

[c] Values in parentheses are for highest-resolution shell.